Bud3 activates Cdc42 to establish a proper growth site in budding yeast

Pil Jung Kang,[1] Mid Eum Lee,[2] and Hay-Oak Park[1,2]

[1]Department of Molecular Genetics and [2]Molecular Cellular Developmental Biology Program, The Ohio State University, Columbus, OH 43210

Cell polarization occurs along a single axis that is generally determined by a spatial cue, yet the underlying mechanism is poorly understood. Using biochemical assays and live-cell imaging, we show that cell polarization to a proper growth site requires activation of Cdc42 by Bud3 in haploid budding yeast. Bud3 catalyzes the release of guanosine diphosphate (GDP) from Cdc42 and elevates intracellular Cdc42–guanosine triphosphate (GTP) levels in cells with inactive Cdc24, which has as of yet been the sole GDP–GTP exchange factor for Cdc42. Cdc42 is activated in two temporal steps in the G1 phase: the first depends on Bud3, whereas subsequent activation depends on Cdc24. Mutational analyses suggest that biphasic activation of Cdc42 in G1 is necessary for assembly of a proper bud site. Biphasic activation of Cdc42 or Rac GTPases may be a general mechanism for spatial cue–directed cell polarization in eukaryotes.

Introduction

Cells of the budding yeast *Saccharomyces cerevisiae* undergo polarized growth in two spatially programmed patterns. Haploid **a** and α cells bud in an axial pattern, in which both mother and daughter cells select a new bud site adjacent to their immediately preceding division site. In contrast, diploid **a**/α cells bud in a bipolar pattern: mother cells choose a bud site adjacent to the division site or at the opposite pole, whereas daughter cells bud preferentially at the pole distal to the division site (Freifelder, 1960; Chant and Pringle, 1995). Each budding pattern depends on distinct cortical markers, which are linked to a common morphogenetic pathway involving Rsr1 (also known as Bud1) and Cdc42. Cdc42 activates its effectors to trigger polarized organization of the actin and septin cytoskeletons and secretion toward the presumptive bud site. Selection of a bud site thus determines the axis of cell polarity (Bi and Park, 2012). Cdc42 is also thought to be involved in bud site selection because overexpression of Cdc42 affects budding patterns and some *cdc42* mutants exhibit bud site selection defects (Johnson and Pringle, 1990; Miller and Johnson, 1997), but the underlying mechanism is unclear.

In the absence of spatial cues, yeast cells can still polarize to a single site, albeit in random orientations. This process, called symmetry breaking, relies on autocatalytic clustering of Cdc42-GTP. A large number of studies have uncovered intricate cross talk among the polarity factors and have suggested positive and negative feedback loops for symmetry breaking. These mechanisms are likely to involve the actin cytoskeleton, the Bem1 complex, and guanine nucleotide dissociation inhibitor (Slaughter et al., 2009; Wu and Lew, 2013), but several critical aspects of symmetry breaking mechanisms and their physiological relevance are under intense debate (Layton et al., 2011; Savage et al., 2012; Freisinger et al., 2013; Slaughter et al., 2013; Smith et al., 2013; Kuo et al., 2014). Furthermore, whether/how these mechanisms are linked to spatial cues is largely unknown.

We investigated the axial budding pattern as a model for spatial cue–directed cell polarization. The axial pattern depends on a transient cortical marker (i.e., the axial landmark) that includes Bud3, Bud4, Axl1, and Axl2 (also known as Bud10; Bi and Park, 2012). The Bud3 and Bud4 protein levels peak in the M phase, and both proteins localize to the mother–bud neck likely through interactions with septins (Chant et al., 1995; Sanders and Herskowitz, 1996). Bud3 and Bud4 interact with each other and recruit Axl1 and Axl2. After cytokinesis, both mother and daughter cells inherit the septins and the axial landmark proteins at the division site in a ring structure, which disassembles around the time when a new septin ring forms (Gao et al., 2007; Kang et al., 2012, 2013). Bud3 contains a putative Dbl homology (DH) domain, which is conserved among

Correspondence to Hay-Oak Park: park.294@osu.edu

Abbreviations used in this paper: DH, Dbl homology; GEF, GDP–GTP exchange factor; MBP, maltose-binding protein; PBD, p21-binding domain; PH, Pleckstrin homology; SC, synthetic complete; TAP, tandem affinity purification; WT, wild type.

The Rockefeller University Press $30.00
J. Cell Biol. Vol. 206 No. 1 19–28
www.jcb.org/cgi/doi/10.1083/jcb.201402040

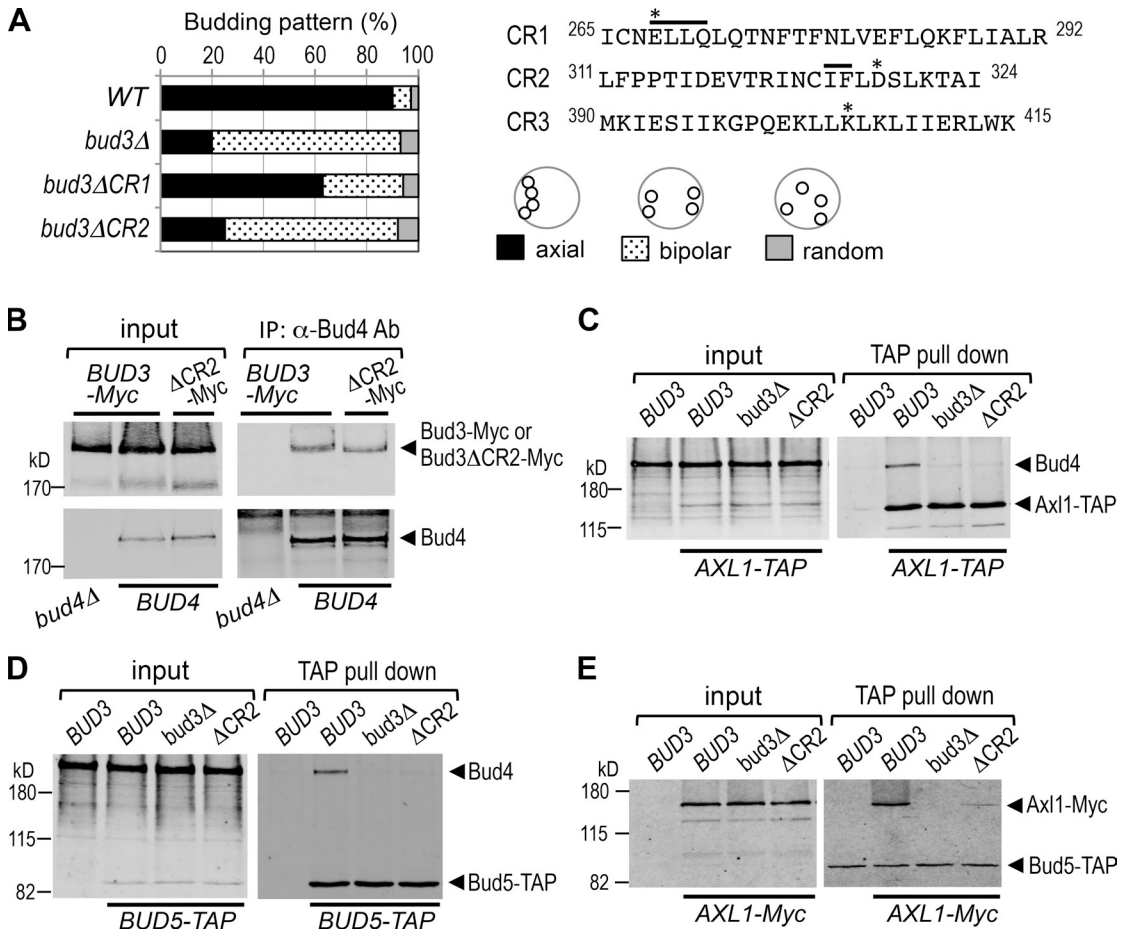

Figure 1. **The Bud3 DH domain is necessary for the axial budding pattern.** (A) Budding pattern (percentage) of haploid *WT*, *bud3Δ*, *bud3ΔCR1*, and *bud3ΔCR2*. The sequences of CR1, CR2, and CR3 are shown. Residues that are deleted or substituted are marked with lines or asterisks, respectively. A mean percentage of each pattern is shown from three independent countings (n = 300; SEM < 3%). An example of bud scar (circles) distribution of each budding pattern is shown. (B) Coimmunoprecipitation of Bud3-Myc or Bud3ΔCR2-Myc with Bud4. The *Bud3-Myc* (either *BUD4* or *bud4Δ*) and *Bud3ΔCR2-Myc* strains were subjected to immunoprecipitation using anti-Bud4 antibodies. Proteins were analyzed by immunoblotting with anti-Myc antibody (top) or anti-Bud4 antibodies (bottom). (C) TAP pull-down assays using the *AXL1-TAP* strains (with either *WT* or a mutant *BUD3* allele) and an untagged strain. After pull-down assays, proteins were analyzed by immunoblotting with anti-Bud4 antibodies. (D and E) TAP pull-down assays using the *BUD5-TAP* (D) and *BUD5-TAP AXL1-Myc* (E) strains with the indicated *BUD3* alleles. The first lane shows a control with untagged *BUD5* (D) or untagged *AXL1* (E). Proteins were analyzed by immunoblotting with anti-Bud4 antibodies (D) or the anti-Myc antibody (E). Ab, antibody; IP, immunoprecipitation.

the Rho GDP–GTP exchange factors (GEFs; Schmidt and Hall, 2002), but it has thus far been unclear whether this domain is functionally significant in axial budding.

Here, we provide evidence that Bud3 activates Cdc42 in early G1 and that this Cdc42 activation is necessary for the assembly of the axial landmark. Our in vitro and in vivo data suggest a new mechanism for spatial cue–directed cell polarization, which involves two step activation of Cdc42 in G1.

Results and discussion

To address the functional significance of the putative DH domain of Bud3, we first introduced deletion and substitution mutations in the conserved regions (CR1–CR3) based on the sequence comparison to the Dbl family of proteins (Fig. 1 A; Aghazadeh et al., 1998). Although most *bud3* mutants exhibited partial defects in the axial budding pattern (Fig. S1 A), *bud3ΔCR2* budded in the same bipolar pattern as cells deleted for *BUD3* (Fig. 1 A). This defect is unlikely caused by protein instability because the Bud3 and Bud3ΔCR2 protein levels were similar (Fig. 1 B).

We then tested whether the *bud3ΔCR2* mutation affects assembly of the axial landmark. When Bud4 was immunoprecipitated, Bud3 and Bud3ΔCR2 were efficiently coprecipitated with Bud4 (Fig. 1 B). Because the Bud4 and septin rings are unstable in *bud3Δ* cells during and after cytokinesis (Kang et al., 2012, 2013), we examined localization of Bud4 and Cdc3 in *bud3ΔCR2* cells and found that these proteins localized normally in cells expressing Bud3ΔCR2 (Fig. S1, B and C). Thus, Bud3ΔCR2 has little defect in interaction with Bud4 or septins. In contrast, Bud4 poorly copurified with Axl1–tandem affinity purification (TAP) in *bud3Δ* and *bud3ΔCR2* cells (Fig. 1 C). Because the interaction between the axial landmark and Bud5 (a GEF for Rsr1) is critical for axial budding (Kang et al., 2001, 2012), we tested whether the *bud3ΔCR2* mutation affects this interaction. When Bud5-TAP was purified, Bud4 and Axl1 poorly associated with Bud5 in *bud3ΔCR2* and *bud3Δ* cells (Fig. 1, D and E). Collectively, these data indicate that the DH

domain of Bud3 is necessary for proper assembly of the axial landmark and thus for the axial budding pattern.

Because the DH domain of Bud3 is functionally important, we wondered whether Bud3 is indeed a GEF, and if so, what its substrate is. We reasoned that if Bud3 functions as a GEF, its substrate would also be necessary for the axial budding pattern. Because Bud4, a GTP-binding protein, is involved in axial budding, we initially considered Bud4 as a potential substrate of Bud3. However, *bud4* mutants that are expected to express Bud4 in the GTP- or GDP-locked (or nucleotide free) state budded in the axial pattern and did not have any obvious defect in association with Axl1, Axl2, and Bud5 (Fig. S2; Kang et al., 2012). Thus, guanine nucleotide exchange of Bud4 is not important for bud site selection, suggesting that Bud4 is not a substrate of Bud3.

We then examined budding patterns of deletion or temperature-sensitive mutants of Rho family GTPases. Surprisingly, *cdc42-101* exhibited the bipolar budding pattern at the semipermissive temperature of 30°C (Fig. 2 A), whereas *cdc42-118* exhibited a mixed budding pattern (Kozminski et al., 2003). Interestingly, the axial budding defect of *cdc42-101* was partially rescued by overexpression of *BUD3* but not by *bud3ΔCR2*. All other *cdc42* and *rho* mutants tested, including *rho4Δ*, exhibited little defects in the axial pattern (Fig. 2 A), although Bud3 homologues in other fungi have been suggested to function as a Rho4 GEF (Justa-Schuch et al., 2010; Si et al., 2010).

Both *cdc42-101* and *cdc42-118* are defective in polarity establishment and thus unable to grow at 37°C (Kozminski et al., 2000). Overexpression of *BUD3* (but not *bud3ΔCR2*) greatly ameliorated the temperature-sensitive growth of *cdc42-101* and slightly that of *cdc42-118* (Fig. 2 B). In contrast, *RSR1* on a multicopy plasmid suppressed *cdc42-118* efficiently but only partially *cdc42-101* (Kozminski et al., 2003). *BUD3* thus appears to be a specific multicopy dosage suppressor of *cdc42-101*. This allele-specific suppression of *cdc42-101* by *BUD3* suggests a functional link between Cdc42 and Bud3.

To explore the possibility that Bud3 functions as a Cdc42 GEF, we first tested by a yeast two-hybrid assay whether Bud3 interacts with Cdc42 in a guanine nucleotide–specific manner because GEFs interact with GDP-bound GTPases and stabilize nucleotide-free intermediates (Schmidt and Hall, 2002). The wild-type (WT) or mutant Cdc42 was expressed as an activation domain fusion, and the Bud3 DH domain was expressed as a DNA-binding domain fusion in a strain carrying the *LEU2* reporter. Cells expressing $Cdc42^{D118A}$ or $Cdc42^{G15A}$, which are expected to be in either a GDP-locked or nucleotide-free state in vivo (Davis et al., 1998; Daubon et al., 2011), grew better on a plate lacking Leu than cells expressing either WT Cdc42 or GTP-locked $Cdc42^{G12V}$ or carrying a vector (Fig. 3 A, top). This two-hybrid interaction was also observed in the *rsr1Δ* host strain (Fig. 3 A, bottom), suggesting that the interaction between Cdc42-GDP and the Bud3 DH domain is not mediated by Rsr1.

We then performed an in vitro binding assay using the purified maltose-binding protein (MBP)–Bud3 truncation (which contains the DH domain) and GST fusions of WT and mutant Cdc42. When each GST-Cdc42 was subjected to a pull-down assay after mixing an equal amount of Bud3, more Bud3 was recovered

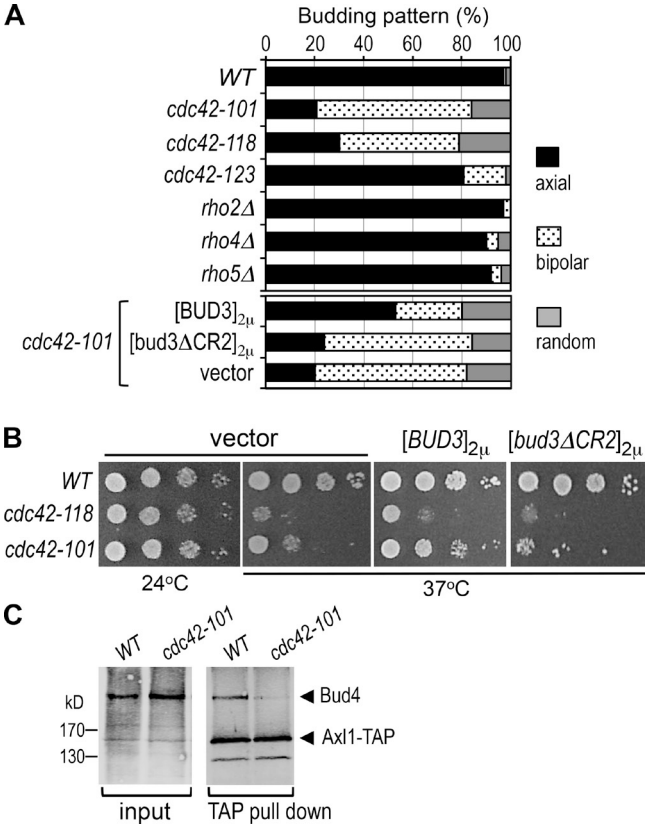

Figure 2. **A *cdc42* mutant is defective in the axial budding pattern.** (A) Budding pattern (percentage) of each haploid strain and *cdc42-101* carrying each plasmid at 30°C. Budding pattern was determined as in Fig. 1 A. (B) 10-fold serial dilutions of *WT* and *cdc42* mutants carrying each plasmid were compared for growth at 24 or 37°C (SC-Ura for 4 d). (C) The *WT* and *cdc42-101* strains expressing *AXL1-TAP* were subjected to TAP purification. Lysates (left) and purified proteins (right) were analyzed by immunoblotting with anti-Bud4 antibodies.

with $Cdc42^{T17N}$ and $Cdc42^{D57Y}$, which are expected to sequester a Cdc42 GEF by analogy to ras^{Asn17} and ras^{Tyr57} (Moskow et al., 2000), than with WT or the dominant-active $Cdc42^{Q61L}$ (Fig. 3 B). These results, together with the two-hybrid interaction, indicate that Bud3 interacts preferentially with Cdc42 in the GDP-bound or nucleotide-free state, consistent with its potential role as a Cdc42 GEF.

Next, we tested directly whether Bud3 could stimulate release of GDP from Cdc42 using Cdc42 preloaded with mant (*N*-methylanthraniloyl)-GDP, a fluorescent GDP analogue, and the MBP-Bud3 fragment. Remarkably, the Bud3 fragment facilitated mant-GDP release from Cdc42 compared with the MBP control (Fig. 3 C). Bud3 exhibited reproducible GEF activity, albeit weak, which was abolished by the *bud3ΔCR2* mutation. In contrast, Bud3 was unable to stimulate mant-GDP release from Rsr1 (Fig. 3 D), suggesting that the effect of Bud3 was specific to Cdc42. These results indicate that Bud3 can function as a Cdc42 GEF in vitro. Unlike most Rho GEFs, which have a tandem DH–Pleckstrin homology (PH) domain, Bud3 lacks a PH domain. This might account for its relatively weak GEF activity. The DH domain interacts with Rho GTPases and mediates the GEF activity, whereas the PH domain appears to have diverse functions, including membrane anchoring or enhancing the catalytic

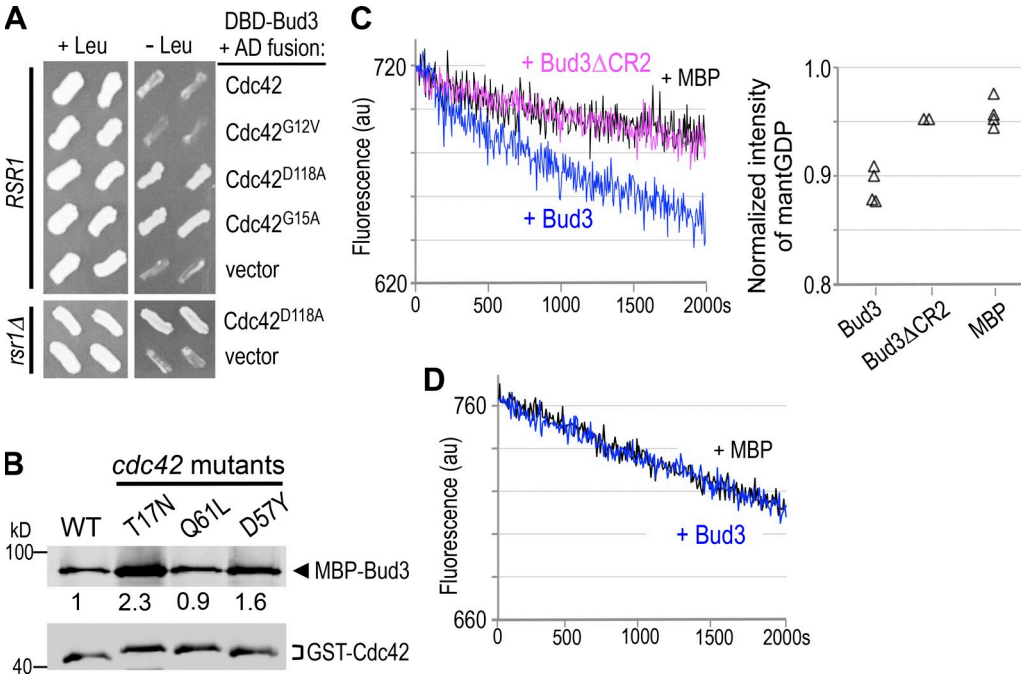

Figure 3. **Bud3 has a GEF activity for Cdc42.** (A) Two-hybrid assays between Cdc42 and Bud3. Two independent transformants of DNA-binding domain (DBD)–Bud3(m) and each activation domain (AD) fusion of WT or mutant Cdc42 or a vector control were patched on SGal-His and Trp (left) or SGal-His, Trp, and Leu (right) in the *RSR1* or *rsr1Δ* host strain and incubated at 25°C for 4–5 d. (B) GST pull-down assays using MBP-Bud3(s) and extracts carrying each GST-Cdc42. Cdc42 and Bud3 were detected with anti-GST and anti-MBP antibodies, respectively. Numbers indicate relative amounts of Bud3 recovered, normalized to its recovery with GST-Cdc42^{WT}. (C) A representative GEF assay using GST-Cdc42 preloaded with mant-GDP. Mant-GDP fluorescence was measured over time after adding an equimolar amount of MBP-Bud3, MBP-Bud3ΔCR2, or MBP. (right) Mant-GDP fluorescence at t = 2,000 s is depicted from independent assays, normalized to the initial fluorescence (at t = 0). (D) A GEF assay using GST-Rsr1 preloaded with mant-GDP and MBP-Bud3 or MBP. Results from two independent assays were almost identical. au, arbitrary unit.

activity of the DH domain (Bos et al., 2007). Bud3 might function more efficiently in vivo by forming a complex with Bud4, which has a putative PH domain, as in the case of the DOCK–ELMO complex, a GEF for Rac (Lu et al., 2004). Further investigation is necessary to test this and other possibilities.

It was surprising to find that Bud3 could stimulate GDP dissociation from Cdc42 because Cdc24 was thought to be the sole Cdc42 GEF in budding yeast. Does Bud3 indeed activate Cdc42 in vivo? To address this question, we monitored Cdc42-GTP levels in a *cdc24^{ts}* mutant using the p21-binding domain (PBD)–RFP (Gic2 PBD fused to tdTomato) as a probe for Cdc42-GTP (Okada et al., 2013). A previous photobleaching study shows that the PBD-GFP clusters fully recover their initial fluorescence intensity in less than a second after photobleaching (Ozbudak et al., 2005). This probe thus responds rapidly to changes in Cdc42-GTP levels. When *cdc24^{ts}* cells that express PBD-RFP and carry a multicopy *BUD3* or *bud3ΔCR2* plasmid or a vector control were shifted to 37°C for 3 h, the majority of these cells were arrested as unbudded cells, as expected from the significant reduction of the Cdc42-GTP level upon temperature upshift (Atkins et al., 2013). Although Bud3 and Bud3ΔCR2 proteins were present at about equal levels, Cdc42-GTP clusters were observed in a larger number of the cells overexpressing Bud3 (39%, n = 128) than in cells with a vector (6.6%, n = 212) or in cells overexpressing Bud3ΔCR2 (1.5%, n = 202; Fig. 4 A). Quantification of PBD-RFP intensity indicated that the Cdc42-GTP levels were not statistically different regardless of whether the clusters arose in cells carrying the BUD3 plasmid or the empty vector. The polarized Cdc42-GTP in cells with the vector might be caused by the Bud3 activity encoded by the chromosomal *BUD3* gene or residual Cdc24 activity remaining after the temperature shift. In contrast, the level of Cdc42-GTP was significantly lower in those few polarized cells with the bud3ΔCR2 plasmid (Fig. 4 A), suggesting that Bud3ΔCR2 might compete with the endogenous Bud3 for Cdc42 association. Together, these results indicate that Bud3 activates Cdc42 in vivo.

Expression of *BUD3* is tightly regulated during the cell cycle, and its constitutive overexpression causes a cytokinesis defect and the formation of extra and abnormally shaped septin rings (Lord et al., 2000). To test whether this phenotype is a result of inappropriate timing and/or level of Cdc42 activation, we monitored Cdc42-GTP in cells overexpressing GFP-Bud3 or GFP-Bud3ΔCR2 from the *GAL* promoter. Cells overexpressing GFP-Bud3 showed an elongated bud shape (Fig. 4 B) and had elevated levels of Cdc42-GTP compared with the cells overexpressing GFP-Bud3ΔCR2 or uninduced cells (Fig. 4 B). We also observed abnormal and extra septin rings in *WT* and *bud4Δ* cells overexpressing Bud3 (Fig. S1 D). Hyperactivation of Cdc42 and/or its activation at an improper time in the cell cycle might have resulted in a prolonged period of apical growth and thus the elongated bud shape. The proper level and/or timing of Bud3 activity is therefore likely to be critical for normal morphogenesis.

When does Bud3 activate Cdc42 in vivo? To closely examine Cdc42 activation in the cell cycle, we performed time-lapse imaging of cells expressing PBD-RFP and Cdc3-GFP (as a marker for cytokinesis) every minute, focusing on the time

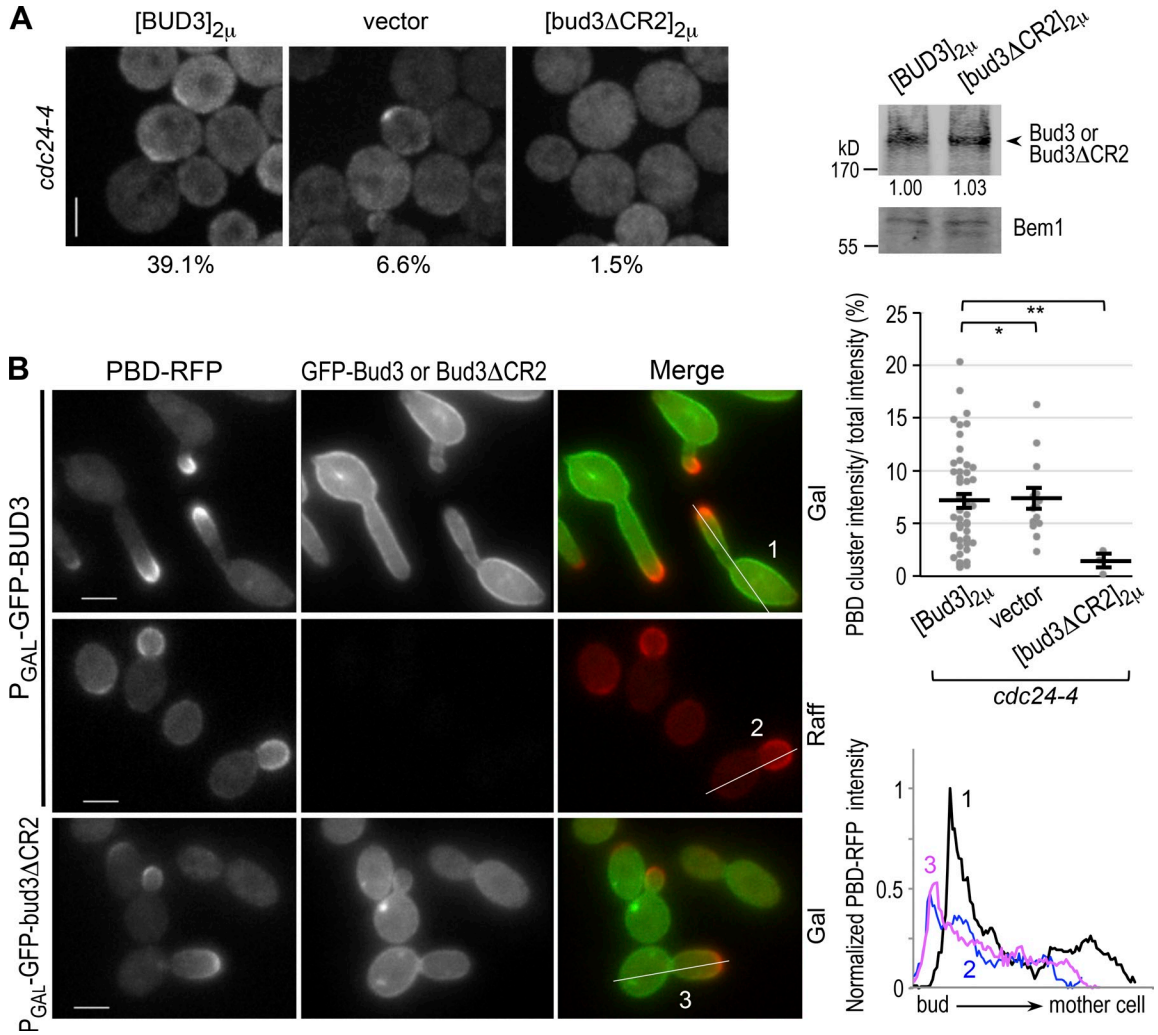

Figure 4. **Bud3 activates Cdc42 in vivo.** (A) PBD-RFP polarization in *cdc24*^{ts} cells carrying each multicopy plasmid after shifting to 37°C for 3 h. Percentages of cells with Cdc42-GTP clusters are shown. (right) The Bud3 and Bud3ΔCR2 protein levels in *cdc24*^{ts} cells carrying each multicopy plasmid. Relative amount of each protein (numbers at bottom) is estimated using Bem1 as a control. (bottom) Quantification of PBD-RFP clusters in individual polarized cells is shown as a percentage of the whole-cell intensity with means (horizontal lines) ± SEM (error bars). *, P = 0.86; **, P < 10^{-3}. (B) Cdc42-GTP polarization in *WT* cells overexpressing GFP-Bud3 or GFP-Bud3ΔCR2 (7 h in galactose [Gal]) or in uninduced cells (raffinose [Raff]). About 79% of medium- or large-budded cells (*n* = 100) overexpressing GFP-Bud3 had elongated buds (a/b [ratio of major and minor axes] > 2; often a/b > 4), whereas <1% of cells overexpressing GFP-Bud3ΔCR2 had elongated buds (*n* = 100). Cells overexpressing GFP-Bud3ΔCR2 had slightly more elongated buds (a/b = ∼1.5) than uninduced cells (a/b = ∼1.2). Line scans show PBD-RFP intensity of numbered cells, normalized to the peak intensity of the cell #1. Bars, 3 µm.

window from M to the next G1. Little Cdc42-GTP was detectable at the onset of cytokinesis (when the Cdc3 ring splits, *t* = 0; Fig. 5) as previously reported (Atkins et al., 2013; Okada et al., 2013). Surprisingly, Cdc42-GTP started to accumulate within 5 min after the onset of cytokinesis at 22°C (100%, *n* = 10; Fig. 5 A and Video 1). Because Myo1 ring contraction takes ∼6–8 min under similar conditions, the result indicates that Cdc42 activation begins in telophase or in early G1 phase. In contrast, when *bud3ΔCR2* cells were imaged under similar conditions, little Cdc42-GTP was observed in early G1, although robust Cdc42-GTP polarization was observed at later time points (100%, *n* = 14; Fig. 5 B and Video 2). This late Cdc42-GTP peak, which appeared at either pole of the *bud3ΔCR2* cells, was approximately concurrent with appearance of the new septin "clouds."

Strikingly, quantification of PBD-RFP clusters in individual mother and daughter cells revealed two temporal steps of Cdc42 activation during G1, although the two steps are less clearly separated in mother cells. In *WT* mother cells, Cdc42-GTP accumulated soon after the onset of cytokinesis, which was immediately followed by the second wave of Cdc42-GTP, despite some fluctuation in its level. In contrast, the first Cdc42-GTP wave was missing in the *bud3ΔCR2* mother cells (Fig. 5 C and Fig. S3 A). The first Cdc42-GTP peak was also evident in *WT* daughter cells, but more time elapsed between the early and the late Cdc42-GTP waves, likely because of their longer G1 phase (Fig. 5 C and Fig. S3 A). Both Cdc42 waves were evident within 25–30 min after the onset of cytokinesis in *WT* daughter cells at 30°C (*n* = 10; Fig. S3, A [c] and B). In the *bud3ΔCR2* daughter cells, only the second Cdc42 activation was observed at 30°C within 30 min after the onset of cytokinesis (*n* = 18; Fig. S3 A, c). Despite cell-to-cell variations in timing of these two Cdc42 peaks, which are likely caused by temporal G1 variability (Di Talia et al., 2007), the mean time interval between the onset of cytokinesis

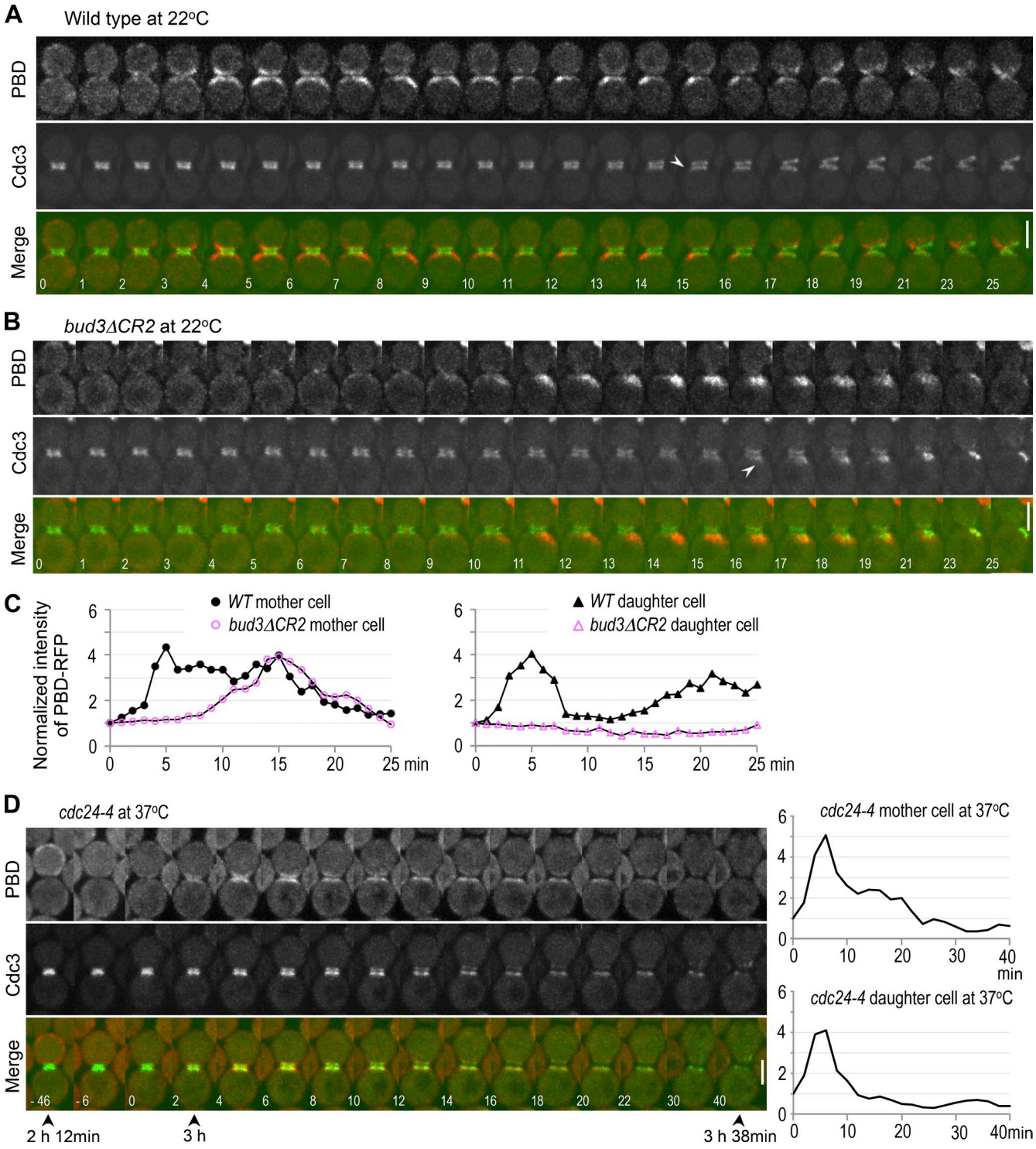

Figure 5. **Bud3 activates Cdc42 in early G1.** (A and B) Time-lapse imaging of PBD-RFP and Cdc3-GFP in *WT* (A) and *bud3ΔCR2* (B) cells at 22°C. Arrowheads mark first appearance of new septins in mother cells. Numbers indicate time (in minutes) from the onset of cytokinesis ($t = 0$). (C) Quantification of PBD-RFP in mother and daughter cells shown in A and B. PBD-RFP intensity is normalized to intensity at $t = 0$. (D) Time-lapse imaging of PBD-RFP and Cdc3-GFP in *cdc24-4* cells every 2 min at 37°C, and selected images are shown. Numbers (white) indicate the time (minutes) relative to the onset of cytokinesis ($t = 0$); numbers (black) below images indicate the time after shifting to 37°C. PBD-RFP intensity is normalized as in C. Bars, 3 µm.

and the appearance of new septin was about the same in *WT* and *bud3ΔCR2* cells (Fig. 5 and Fig. S3 A). The absence of the first Cdc42-GTP wave in *bud3ΔCR2* cells is thus likely a result of the lack of Bud3 GEF activity rather than different length of the G1 phase.

This stepwise activation of Cdc42 in G1 may be related to the temporal G1 regulation. The G1 phase is partitioned into two temporal steps by nuclear exit of the transcriptional repressor Whi5: the first step depends on the G1 cyclin Cln3 and the second step depends on the late G1 cyclin Cln1/Cln2 (Di Talia

et al., 2007; Skotheim et al., 2008). Once Whi5 exits from the nucleus, Swi4–Swi6 and Mbp1–Swi6 activate transcription of hundreds of genes, including *CLN1* and *CLN2*. Indeed, the two Cdc42-GTP waves were temporally separated by the exit of Whi5 from the nucleus in daughter cells (Fig. S3 C). This separation of Cdc42-GTP waves was not detectable in mother cells at 30°C, likely because of immediate Cdc24 activation in mother cells, which have achieved the minimum cell size in their first cell division and thus have very short T1 (the period between cytokinesis and Whi5 exit). Cdc24 is sequestered within the nucleus in haploid cells during G1 (Toenjes et al., 1999; Nern and Arkowitz, 2000; Shimada et al., 2000), and its relocation to the presumptive bud site depends on activation of the late G1 Cdk (Gulli et al., 2000; Moffat and Andrews, 2004). The second Cdc42-GTP wave is thus likely caused by activation by Cdc24. Consistent with this idea, when we imaged *cdc24^{ts}* cells expressing PBD-RFP after temperature upshift to 37°C, the first Cdc42-GTP peak appeared transiently in early G1, but the second Cdc42-GTP peak was not observed (100%, $n = 9$; Fig. 5 D).

What would necessitate activation of Cdc42 by Bud3? Because we found a *cdc42* mutant with a specific defect in the axial pattern at 30°C (Fig. 2 A), we wondered whether Cdc42 might function in the assembly of the axial landmark upon activation by Bud3. To test this idea, we examined interaction between Bud4 and Axl1 in the *cdc42-101* mutant, which was grown at 30°C. Indeed, Axl1-TAP poorly associated with Bud4 in *cdc42-101* cells, unlike in *WT* cells (Fig. 2 C), suggesting that Cdc42 is necessary for the assembly or stability of the axial landmark. It is not clear yet whether cycling of Cdc42 between the GTP- and GDP-bound state is directly involved in the assembly of the axial landmark or whether a Cdc42 effector might be involved in assembly of the axial landmark and subsequent bud site assembly. Further investigation is necessary to test these or other models.

In conclusion, we provide evidence for two temporal steps of Cdc42 activation in G1: the first depends on Bud3, whereas subsequent activation depends on Cdc24. We propose that this sequential activation of Cdc42 governs recognition of spatial landmarks and execution of polarity establishment. Robust Cdc42 activation in late G1 is likely to be controlled by positive feedback mechanisms, as suggested by several previous studies (Butty et al., 2002; Irazoqui et al., 2003; Wedlich-Soldner et al., 2004; Goryachev and Pokhilko, 2008; Kozubowski et al., 2008). Because Rsr1 is linked to the axial landmark via Bud5 (Kang et al., 2001; Marston et al., 2001), a potential positive feedback circuit that includes Bud3 and the Rsr1 GTPase module might be involved in activation of Cdc42 in early G1. Interestingly, biphasic activation of Rac and Cdc42 GTPases has been observed during spatial cue–directed cell polarization in growth factor–stimulated endothelial cells or antigen-stimulated mast cells, and this mechanism often involves early transient and late sustained activation phases (El-Sibai and Backer, 2007; Garrett et al., 2007; Kobayashi et al., 2011). Thus, biphasic activation may represent a general mechanism underlying spatial cue–dependent cell polarization.

Materials and methods

DNA manipulation, genetic methods, and growth conditions

Standard methods of yeast genetics, DNA manipulation, and growth conditions were used (Guthrie and Fink, 1991), unless indicated otherwise. Synthetic complete (SC) media with a specific supplement dropped out (such as SC-Ura) were used to maintain plasmids. All media contained 2% dextrose as a carbon source, except where indicated, 2% galactose (SGal) or 2% raffinose (SRaf) was used instead of dextrose. Specific mutations were introduced by PCR (see following paragraphs) and confirmed by DNA sequencing. The strains, plasmids, and oligonucleotides used in this study are listed in Tables S1–S3.

Site-directed mutagenesis of the DH domain of *BUD3* was performed by PCR, essentially as previously described (Kang et al., 2012). First, pRS425-BUD3 was generated by inserting the BamHI–SalI fragment (covering 608 bp upstream and 406 bp downstream of the *BUD3* ORF) from p13 (Chant et al., 1995) into pRS425. The *bud3^{E268A}* and *bud3^{K405S}* mutations were generated by PCR using pRS425-BUD3 as a template and primer pairs of oBUD33 and oBUD34 and oBUD35 and oBUD36. To generate the *bud3$^{E268A,\ K405S}$* mutation, the 490-bp BglII–SphI fragment of pRS425-bud3^{K405S} was replaced with the BglII–SphI fragment of pRS425-bud3^{E268A}, yielding pRS425-bud3$^{E268A,\ K405S}$.

The *bud3ΔCR1* and *bud3ΔCR2* mutations were generated by two-step PCR strategy. First, separate PCR reactions were performed using pRS425-BUD3 as a template and primer pair oBUD39 and oBUD311 and primer pair oBUD32 and oBUD312 for *bud3ΔCR1*. Primer pair oBUD39 and oBUD313 and primers oBUD32 and oBUD314 were used for *bud3ΔCR2*. These PCR products were ligated together after PstI digestion and then used as templates in the second PCR reactions with primers oBUD39 and oBUD32. The resulting products were digested with BglII and SphI and then used to replace the 490-bp BglII–SphI fragment of pRS425-BUD3, yielding pRS425-bud3ΔCR1 and pRS425-bud3ΔCR2.

An integrating plasmid pRS305-BUD3 covers 2.82 kb upstream (native BglII site) and 406 bp downstream (SalI site) of the *BUD3* ORF. Plasmids pRS305-bud3ΔCR1 and pRS305-bud3ΔCR2 were constructed by the replacement the 2.8-kb BglII–XhoI fragment of pRS305-BUD3 with those of pRS425-bud3ΔCR1 and pRS425-bud3ΔCR2. These pRD305-BUD3 plasmids were linearized with BamHI digestion for chromosomal integration. Additional 2μ plasmids, pRS426-BUD3 and pRS426-bud3ΔCR2, were constructed by inserting the 5.8-kb BamHI–SalI fragment from pRS425-BUD3 or pRS425-bud3ΔCR2 into pRS426.

To generate an MBP fusion of Bud3 (aa 211–498) or Bud3ΔCR2 (aa 211–498), first, DNA fragments encoding WT Bud3 and Bud3ΔCR2 were generated by PCR using primer pair oBUD31 and oBUD315 and primer pair pRS425-BUD3 and pRS305-bud3ΔCR2, respectively, as templates. These PCR products were digested with BamHI and HindIII and then cloned into pMALc2 digested with the same enzymes, yielding pMAL-c2-Bud3(s) (aa 211–498) and pMAL-c2-bud3ΔCR2(s) (aa 211–498).

Site-directed mutagenesis of *BUD4* was performed by PCR as previously described (Kang et al., 2012). Specifically, the *bud4$^{T1183N,\ K1183S}$* mutation was generated by two-step PCR strategy. First, separate PCR reactions were performed using pRS304-BUD4 (Kang et al., 2012) as a template and primers oBUD410 and oBUD412 and primers oBUD47 and oBUD411. The PCR products were ligated together after EcoRI digestion and then used as template in the second PCR with primers oBUD47 and oBUD412. The resulting product was digested with AatII and AgeI and then replaced with the 1.64-kb AatII–AgeI fragment of pRS304-BUD4, yielding pRS304-bud4$^{T1182N,\ K1183S}$. The *bud4^{D1403A}* mutation was introduced by PCR-based site-directed mutagenesis using pRS304-BUD4 as a template and primers oBUD413 and oBUD414.

Yeast two-hybrid assays

The WT and mutant Cdc42 were expressed as activation domain fusion proteins using pJG4-5 (Gyuris et al., 1993). All Cdc42 constructs also carry the C188S mutation to avoid membrane targeting, and thus, overexpression of these *CDC42* mutants does not affect cell viability (Fig. 3 A, right). To introduce the *cdc42^{G15A}* mutation, two-step PCR strategy was used. First, separate PCR reactions were performed using pEG202-cdc42^{C188S} as a template and primers oPEG202UP and oCDC42G15A-2 and primers oPEG202DOWN and oCDC42G15A-1. Both PCR products were used in the second fusion PCR with primers oPEG202UP and oPEG202DOWN. The resulting product was digested with EcoRI and XhoI and then ligated with the EcoRI–XhoI-digested vector pEG202, yielding pEG202-cdc42$^{G15A,\ C188S}$. This *cdc42* mutant was cloned into pJG4-5 by inserting the 600-bp EcoRI–XhoI fragment of pEG202-cdc42$^{G15A,\ C188S}$ into the EcoRI–XhoI-digested vector pJG4-5,

yielding pJG4-5–cdc42$^{G15A,\ C188S}$. Similarly, pJG4-5–cdc42$^{D118A,\ C188S}$ was generated from pEG202-cdc42$^{D118A,\ C188S}$ (gift from M. Peter, Eidgenössische Technische Hochschule Zürich, Zürich, Switzerland). Plasmids pJG4-5–cdc42^{C188S} and pJG4-5–cdc42$^{G12V,\ C188S}$ were provided by M. Peter (Butty et al., 2002). To express the Bud3 DH domain as a DNA-binding domain fusion, the N-terminal Bud3 fragment (aa 1–656) was cloned into pEG202 in the following steps: First, a PCR reaction was performed using pRS425-BUD3 as a template and primers oBUD332 and oBUD333. After digestion with EcoRI and XhoI, the PCR fragment was ligated into pEG202 digested with the same enzymes, yielding pEG202-Bud3(m) (aa 1–656). Two-hybrid assays were performed using the *LEU2* reporter in *WT* (EGY48) or *rsr1Δ* (HPY2623) strains.

Budding pattern

Bud scars of *cdc42* mutants (provided by K. Kozminski, University of Virginia, Charlottesville, VA; Kozminski et al., 2000) and *rho* mutants (GE Healthcare) were visualized by staining cells with Calcofluor as previously described (Pringle, 1991). Cells were grown overnight at 30°C in YPD (yeast extract, peptone, dextrose), unless cells were carrying a plasmid, when synthetic dropout medium was used. Cells with more than three bud scars were counted, and a mean percentage of each budding pattern was indicated from three independent countings.

Protein expression and purification

Cdc42 and Rsr1 were expressed as a GST fusion protein in *Escherichia coli* using plasmid pDLB2091 (a gift from D. Lew, Duke University, Durham, NC; Gladfelter et al., 2002) and plasmid pRS4 (Holden et al., 1991), respectively. The Bud3 fragment (aa 211–498) and the same fragment carrying the *bud3ΔCR2* mutation were expressed as MBP fusion proteins in *E. coli* using plasmids pMAL-c2-Bud3(s) and pMAL-c2-bud3ΔCR2(s), respectively. These proteins were purified from a protease-deficient *E. coli* strain (BL21-CodonPlus), as previously described (Kozminski et al., 2003). In brief, after harvesting cells, the cell pellet was resuspended in PBS containing 200 µg/ml lysozyme, 0.1% Triton X-100, 1 mM DTT, 1 mM EDTA, 1 mM EGTA, 1 mM PMSF, and 2 mM benzamidine hydrochloride. Cells were lysed by freeze and thaw and by brief sonication. Cell extracts were then centrifuged for 30 min at 12,000 *g*, and the clear supernatant was loaded on the column for affinity purification. The protein concentration was estimated by Coomassie blue staining with protein standards after SDS-PAGE.

Immunoprecipitation, immunoblotting, and in vitro binding assays

All yeast strains including *cdc42-101* were grown to mid–log phase (OD_{600} of ∼1.0) in YPD at 30°C. Immunoprecipitation and IgG-agarose pull-down assays were performed at 4°C (except where noted), essentially as previously described (Kang et al., 2012). In brief, 70–100 OD_{600} units of cells were used to prepare cell lysates using a lysis buffer (50 mM Hepes, pH 7.6, 300 mM KCl, 1 mM EGTA, 1 mM $MgCl_2$, 10% glycerol, and 1% Triton X-100) with a cocktail of protease inhibitors. The crude cell lysates were centrifuged for 12 min at 10,000 *g*, and the supernatant (S10 fraction) was used for subsequent assays. The S10 fraction was incubated with 1 µl anti-Bud4 antiserum on ice (with occasional mixing) for 1 h and then incubated with 25 µl protein A–agarose beads (Roche) for 40 min. For pull-down assays, the S10 fraction was incubated with 25 µl IgG-Sepharose beads (GE Healthcare) for 1 h at 4°C by rocking. After washing with the same lysis buffer, proteins were eluted from protein A–agarose beads or IgG-Sepharose beads and then subjected to immunoblotting. Myc-, GST-, MBP-, and TAP-tagged proteins were detected using anti-Myc antibody 9E10 (provided by M. Bishop, University of California, San Francisco, San Francisco, CA), rabbit anti-GST antibody (Santa Cruz Biotechnology, Inc.), rabbit anti-MBP antibody (New England Biolabs, Inc.), and rabbit monoclonal anti-calmodulin–binding protein (EMD Millipore), respectively. Bud4, Bud3, and Bem1 were detected using polyclonal antibodies against Bud4, Bud3 (provided by M.S. Longtine, Washington University in St. Louis, St Louis, MO), and Bem1 (gift from J.R. Pringle, Stanford University, Palo Alto, CA), respectively. These antisera were prepared in rabbits using GST-Bud4 (aa 1–398; Kang et al., 2012), GST-Bud3 (aa 1,111–1,475), and two-thirds of the C-terminal Bem1 fused to β-galactosidase (Pringle et al., 1995). Note that anti-Bud4 antibodies also cross react with Axl1-TAP or Bud5-TAP, owing to the IgG-binding protein segment in TAP. Protein bands were then detected with Alexa Fluor 680 goat anti–rabbit IgG (Molecular Probes) or IRDye 800CW–conjugated goat anti–mouse IgG (LI-COR Biosciences) secondary antibodies using the Odyssey system (LI-COR Biosciences). Proteins were quantified using the software of the Odyssey system.

To determine interaction between GST-Cdc42 fusions and MBP-Bud3, in vitro binding assays were performed as previously described (Kozminski et al., 2003) with slight modifications. In brief, extracts were prepared using lysis buffer (PBS, pH 8.1, 1% Triton X-100, and 10% glycerol) from 100 OD_{600} units of *bud3Δ* cells (HPY2446) carrying each GST-CDC42 plasmid (gift from E. Bi, University of Pennsylvania, Philadelphia, PA; Gao et al., 2007). Each GST-Cdc42 was pulled down using glutathione–agarose beads (Thermo Fisher Scientific) and then incubated with 5 µg of purified MBP-Bud3 (aa 211–498) for 1 h at 4°C. After GST pull-down assays, recovered proteins were analyzed by immunoblotting, as described in the previous paragraph.

In vitro GEF assays

Either GST-Cdc42 or GST-Rsr1 was incubated with 50-fold molar excess of mant-GDP (Invitrogen) in a nucleotide-loading buffer (20 mM Tri-HCl, pH 7.5, 50 mM NaCl, 5 mM EDTA, and 2 mM DTT) for 25 min at 25°C. After terminating the nucleotide loading with $MgCl_2$ (to a final of 20 mM), excess mant-GDP was removed by centrifugation in a filter unit (Microcon YM-10; EMD Millipore), and mant-GDP–loaded GST-Cdc42 or GST-Rsr1 was concentrated in a GEF assay buffer (20 mM Tri-HCl, pH 7.5, 50 mM NaCl, 10 mM $MgCl_2$, 1% glycerol, and 1 mM DTT). A GEF assay was performed by mixing an equimolar amount (∼2 µM) of mant-GDP–loaded Cdc42 or Rsr1 with an equimolar amount of MBP-Bud3 (aa 211–498), MBP-Bud3ΔCR2, or MBP in the GEF assay buffer containing 200 µM GDP. Fluorescence was monitored at 25°C every 4 s for 2,000 s using a fluorescence spectrophotometer (Cary Eclipse; Varian) with excitation at 360 nm and emission at 440 nm.

Microscopy and image analysis

Cells were grown in synthetic medium with dextrose, unless indicated otherwise, overnight and freshly subcultured for 3–4 h in the same medium. Cells were then harvested and mounted on a slab containing the same medium and 2% agarose. The slab was put on a stage directly (at 22°C) or in a temperature-control chamber set to 30 or 37°C, as indicated. For two-color time-lapse imaging, images were captured every min at 22°C or every 2 min at 30°C using a spinning-disk confocal microscope (UltraVIEW VoX CSU-X1 system; PerkinElmer) equipped with a 100×, 1.4 NA Plan Apochromat objective lens (Nikon), 440-, 488-, 515-, and 561-nm solid-state lasers (Modular Laser System 2.0; PerkinElmer), and a back-thinned electron-multiplying charge-coupled device camera (ImagEM C9100-13; Hamamatsu Photonics) on an inverted microscope (Ti-E; Nikon). Time-lapse imaging of the *cdc24-4* mutant was performed similarly, except for the following: cells were grown overnight at room temperature, diluted to prewarmed media (37°C), and shaken for 2 h at 37°C before imaging every 2 min on a slab placed in a temperature-controlled chamber at 37°C.

Maximum intensity projections were generated using UltraVIEW VoX software to generate figures and videos. To quantify fluorescence intensity of PBD-RFP clusters, mean projections were generated from three z sections (spaced at 0.3 µm), and then, a threshold method was used after background subtraction using ImageJ software (National Institutes of Health) as previously described (Okada et al., 2013). The sum of all pixels in either mother or daughter cells was analyzed separately from the onset of cytokinesis until bud emergence (in mother cells), and intensity at each time point was normalized to the intensity at the onset of cytokinesis ($t = 0$). Because of cell-to-cell variations of the G1 length as previously reported (Di Talia et al., 2007), we showed a representative normalized intensity of individual cells instead of averaging them at each time point (Fig. 5 and Fig. S3).

To test whether cells that had depleted Cdc24 activity could polarize Cdc42-GTP, *cdc24^{ts}* cells that express PBD-tdTomato and carry either a multicopy BUD3 plasmid, a multicopy bud3ΔCR2 plasmid, or a vector control were grown at room temperature overnight and then shifted to 37°C for 3 h before imaging. Cells on a slab placed in a temperature-control chamber at 37°C were imaged (nine z sections spaced at 0.3 µm) using the same spinning-disk confocal microscope (UltraVIEW VoX CSU-X1 system) equipped with a 100×, 1.4 NA Plan Apochromat objective lens. To count cells with polarized Cdc42-GTP, unbudded cells that had a PBD-RFP cluster were identified by a threshold method using ImageJ software. The percentage of cells with polarized Cdc42-GTP cap was shown below each image (n = 130–200) in Fig. 4 A. To quantify fluorescence intensity of the PBD-RFP cluster in individual polarized cells, fluorescence thresholds were set to capture either a PBD-RFP cluster or the whole cell, and summed fluorescence intensity was measured using ImageJ software from summed images after background subtraction (background was estimated from the mean whole-cell fluorescence of an untagged strain). Summed fluorescence intensity of a PBD-RFP cluster was divided by the summed intensity in

the whole cell, multiplied by 100 to calculate the fraction of the polarized PBD-RFP, and plotted for each individual polarized cell (Fig. 4 A).

Images in Fig. 4 B and Fig. S1 were captured at 24°C using a microscope (E800; Nikon) fitted with a 100×, 1.3 NA oil Plan Fluor objective lens (Nikon) and FITC/GFP, CFP, and mCherry/Texas red filters obtained from Chroma Technology Corp., a charge-coupled device camera (ORCA-ER; Hamamatsu Photonics), and SlideBook software (Intelligent Imaging Innovations). Where indicated, images were deconvolved using SlideBook software, and maximum intensity projections were generated to make the figures (Fig. S1 D, top).

Overexpression of *BUD3* or *GFP-BUD3*

To overexpress Bud3, GFP-BUD3, or GFP-Bud3ΔCR2 from the *GAL1* promoter, cells were grown in 2% raffinose-containing media first (uninduced) and then induced for 6–7 h after adding galactose (to final 2%) before imaging. Fluorescence intensity of PBD-RFP in these cells was compared by line scan using mean intensity projections of three z sections (n = 80–100). Relative intensities of representative cells, normalized against the maximum pixel intensity, are shown in Fig. 4 B. *BUD3* overexpression was also examined in the *BUD4* and *bud4Δ* strains expressing Cdc3-mCherry from the *GAL1* promoter on a CEN (centromere)-based plasmid (Fig. S1 D).

Statistical analysis

Data analysis was performed with Excel (Microsoft). Statistical differences between two sets of data were determined by a two-tailed Student's *t* test.

Online supplemental material

Fig. S1 shows characterization of *bud3* DH domain mutants. Fig. S2 shows characterization of the GDP-locked (or nucleotide free) forms of Bud4. Fig. S3 shows quantification of PBD-RFP and time-lapse imaging of PBD-RFP and Whi5-GFP at 30°C. Videos 1 and 2 show time-lapse imaging of Gic2-PBD-RFP and Cdc3-GFP in haploid *WT* (Video 1) and *bud3ΔCR2* cells (Video 2) at 22°C. Video 3 shows time-lapse imaging of Gic2-PBD-RFP and Cdc3-GFP in *cdc24-4* cells at 37°C. Table S1 shows yeast strains used in this study. Table S2 shows plasmids used in this study. Table S3 shows oligonucleotides used in this study. Online supplemental material is available at http://www.jcb.org/cgi/content/full/jcb.201402040/DC1. Additional data are available in the JCB DataViewer at http://dx.doi.org/10.1083/jcb.201402040.dv.

We thank K. Kozminski, E. Bi, M. Peter, M.S. Longtine, J.R. Pringle, and D. Lew for antibodies, strains, and plasmids; S. Okada and E. Bi for their help with an ImageJ script; and J. Hood-DeGrenier and L. Huang for comments on the manuscript.

This work was partly supported by a grant from the National Institutes of Health/National Institute of General Medical Sciences to H.-O. Park.

The authors declare no competing financial interests.

Submitted: 10 February 2014
Accepted: 3 June 2014

References

Aghazadeh, B., K. Zhu, T.J. Kubiseski, G.A. Liu, T. Pawson, Y. Zheng, and M.K. Rosen. 1998. Structure and mutagenesis of the Dbl homology domain. *Nat. Struct. Biol.* 5:1098–1107. http://dx.doi.org/10.1038/4209

Atkins, B.D., S. Yoshida, K. Saito, C.-F. Wu, D.J. Lew, and D. Pellman. 2013. Inhibition of Cdc42 during mitotic exit is required for cytokinesis. *J. Cell Biol.* 202:231–240. http://dx.doi.org/10.1083/jcb.201301090

Bi, E., and H.-O. Park. 2012. Cell polarization and cytokinesis in budding yeast. *Genetics*. 191:347–387. http://dx.doi.org/10.1534/genetics.111.132886

Bos, J.L., H. Rehmann, and A. Wittinghofer. 2007. GEFs and GAPs: critical elements in the control of small G proteins. *Cell*. 129:865–877. http://dx.doi.org/10.1016/j.cell.2007.05.018

Butty, A.-C., N. Perrinjaquet, A. Petit, M. Jaquenoud, J.E. Segall, K. Hofmann, C. Zwahlen, and M. Peter. 2002. A positive feedback loop stabilizes the guanine-nucleotide exchange factor Cdc24 at sites of polarization. *EMBO J.* 21:1565–1576. http://dx.doi.org/10.1093/emboj/21.7.1565

Chant, J., and J.R. Pringle. 1995. Patterns of bud-site selection in the yeast *Saccharomyces cerevisiae*. *J. Cell Biol.* 129:751–765. http://dx.doi.org/10.1083/jcb.129.3.751

Chant, J., M. Mischke, E. Mitchell, I. Herskowitz, and J.R. Pringle. 1995. Role of Bud3p in producing the axial budding pattern of yeast. *J. Cell Biol.* 129:767–778. http://dx.doi.org/10.1083/jcb.129.3.767

Daubon, T., R. Buccione, and E. Génot. 2011. The Aarskog-Scott syndrome protein Fgd1 regulates podosome formation and extracellular matrix remodeling in transforming growth factor β-stimulated aortic endothelial cells. *Mol. Cell. Biol.* 31:4430–4441. http://dx.doi.org/10.1128/MCB.05474-11

Davis, C.R., T.J. Richman, S.B. Deliduka, J.O. Blaisdell, C.C. Collins, and D.I. Johnson. 1998. Analysis of the mechanisms of action of the *Saccharomyces cerevisiae* dominant lethal cdc42G12V and dominant negative cdc42D118A mutations. *J. Biol. Chem.* 273:849–858. http://dx.doi.org/10.1074/jbc.273.2.849

Di Talia, S., J.M. Skotheim, J.M. Bean, E.D. Siggia, and F.R. Cross. 2007. The effects of molecular noise and size control on variability in the budding yeast cell cycle. *Nature*. 448:947–951. (published erratum appears in *Nature.* 2007. 450:1272) http://dx.doi.org/10.1038/nature06072

El-Sibai, M., and J.M. Backer. 2007. Phospholipase C gamma negatively regulates Rac/Cdc42 activation in antigen-stimulated mast cells. *Eur. J. Immunol.* 37:261–270. http://dx.doi.org/10.1002/eji.200635875

Freifelder, D. 1960. Bud position in *Saccharomyces cerevisiae*. *J. Bacteriol.* 80:567–568.

Freisinger, T., B. Klünder, J. Johnson, N. Müller, G. Pichler, G. Beck, M. Costanzo, C. Boone, R.A. Cerione, E. Frey, and R. Wedlich-Söldner. 2013. Establishment of a robust single axis of cell polarity by coupling multiple positive feedback loops. *Nat. Commun.* 4:1807. http://dx.doi.org/10.1038/ncomms2795

Gao, X.D., L.M. Sperber, S.A. Kane, Z. Tong, A.H. Tong, C. Boone, and E. Bi. 2007. Sequential and distinct roles of the cadherin domain-containing protein Axl2p in cell polarization in yeast cell cycle. *Mol. Biol. Cell*. 18:2542–2560. http://dx.doi.org/10.1091/mbc.E06-09-0822

Garrett, T.A., J.D. Van Buul, and K. Burridge. 2007. VEGF-induced Rac1 activation in endothelial cells is regulated by the guanine nucleotide exchange factor Vav2. *Exp. Cell Res.* 313:3285–3297. http://dx.doi.org/10.1016/j.yexcr.2007.05.027

Gladfelter, A.S., I. Bose, T.R. Zyla, E.S.G. Bardes, and D.J. Lew. 2002. Septin ring assembly involves cycles of GTP loading and hydrolysis by Cdc42p. *J. Cell Biol.* 156:315–326. http://dx.doi.org/10.1083/jcb.200109062

Goryachev, A.B., and A.V. Pokhilko. 2008. Dynamics of Cdc42 network embodies a Turing-type mechanism of yeast cell polarity. *FEBS Lett.* 582:1437–1443. http://dx.doi.org/10.1016/j.febslet.2008.03.029

Gulli, M.P., M. Jaquenoud, Y. Shimada, G. Niederhäuser, P. Wiget, and M. Peter. 2000. Phosphorylation of the Cdc42 exchange factor Cdc24 by the PAK-like kinase Cla4 may regulate polarized growth in yeast. *Mol. Cell*. 6:1155–1167. http://dx.doi.org/10.1016/S1097-2765(00)00113-1

Guthrie, C., and G. Fink, editors. 1991. *Guide to yeast genetics and molecular biology.* Methods in Enzymology. Vol. 194. Academic Press, San Diego.

Gyuris, J., E. Golemis, H. Chertkov, and R. Brent. 1993. Cdi1, a human G1 and S phase protein phosphatase that associates with Cdk2. *Cell*. 75:791–803. http://dx.doi.org/10.1016/0092-8674(93)90498-F

Holden, J.L., M.S. Nur-E-Kamal, L. Fabri, E. Nice, A. Hammacher, and H. Maruta. 1991. Rsr1 and Rap1 GTPases are activated by the same GTPase-activating protein and require threonine 65 for their activation. *J. Biol. Chem.* 266:16992–16995.

Irazoqui, J.E., A.S. Gladfelter, and D.J. Lew. 2003. Scaffold-mediated symmetry breaking by Cdc42p. *Nat. Cell Biol.* 5:1062–1070. http://dx.doi.org/10.1038/ncb1068

Johnson, D.I., and J.R. Pringle. 1990. Molecular characterization of CDC42, a *Saccharomyces cerevisiae* gene involved in the development of cell polarity. *J. Cell Biol.* 111:143–152. http://dx.doi.org/10.1083/jcb.111.1.143

Justa-Schuch, D., Y. Heilig, C. Richthammer, and S. Seiler. 2010. Septum formation is regulated by the RHO4-specific exchange factors BUD3 and RGF3 and by the landmark protein BUD4 in *Neurospora crassa*. *Mol. Microbiol.* 76:220–235. http://dx.doi.org/10.1111/j.1365-2958.2010.07093.x

Kang, P.J., A. Sanson, B. Lee, and H.-O. Park. 2001. A GDP/GTP exchange factor involved in linking a spatial landmark to cell polarity. *Science*. 292:1376–1378. http://dx.doi.org/10.1126/science.1060360

Kang, P.J., E. Angerman, C.H. Jung, and H.-O. Park. 2012. Bud4 mediates the cell-type-specific assembly of the axial landmark in budding yeast. *J. Cell Sci.* 125:3840–3849. http://dx.doi.org/10.1242/jcs.103697

Kang, P.J., J.K. Hood-DeGrenier, and H.-O. Park. 2013. Coupling of septins to the axial landmark by Bud4 in budding yeast. *J. Cell Sci.* 126:1218–1226. http://dx.doi.org/10.1242/jcs.118521

Kobayashi, H., Y. Ogura, M. Sawada, R. Nakayama, K. Takano, Y. Minato, Y. Takemoto, E. Tashiro, H. Watanabe, and M. Imoto. 2011. Involvement of 14-3-3 proteins in the second epidermal growth factor-induced wave of Rac1 activation in the process of cell migration. *J. Biol. Chem.* 286:39259–39268. http://dx.doi.org/10.1074/jbc.M111.255489

Kozminski, K.G., A.J. Chen, A.A. Rodal, and D.G. Drubin. 2000. Functions and functional domains of the GTPase Cdc42p. *Mol. Biol. Cell*. 11:339–354. http://dx.doi.org/10.1091/mbc.11.1.339

Kozminski, K.G., L. Beven, E. Angerman, A.H.Y. Tong, C. Boone, and H.-O. Park. 2003. Interaction between a Ras and a Rho GTPase couples selection of a growth site to the development of cell polarity in yeast. *Mol. Biol. Cell*. 14:4958–4970. http://dx.doi.org/10.1091/mbc.E03-06-0426

Kozubowski, L., K. Saito, J.M. Johnson, A.S. Howell, T.R. Zyla, and D.J. Lew. 2008. Symmetry-breaking polarization driven by a Cdc42p GEF-PAK complex. *Curr. Biol.* 18:1719–1726. http://dx.doi.org/10.1016/j.cub.2008.09.060

Kuo, C.C., N.S. Savage, H. Chen, C.F. Wu, T.R. Zyla, and D.J. Lew. 2014. Inhibitory GEF phosphorylation provides negative feedback in the yeast polarity circuit. *Curr. Biol.* 24:753–759. http://dx.doi.org/10.1016/j.cub.2014.02.024

Layton, A.T., N.S. Savage, A.S. Howell, S.Y. Carroll, D.G. Drubin, and D.J. Lew. 2011. Modeling vesicle traffic reveals unexpected consequences for Cdc42p-mediated polarity establishment. *Curr. Biol.* 21:184–194. http://dx.doi.org/10.1016/j.cub.2011.01.012

Lord, M., M.C. Yang, M. Mischke, and J. Chant. 2000. Cell cycle programs of gene expression control morphogenetic protein localization. *J. Cell Biol.* 151:1501–1512. http://dx.doi.org/10.1083/jcb.151.7.1501

Lu, M., J.M. Kinchen, K.L. Rossman, C. Grimsley, C. deBakker, E. Brugnera, A.C. Tosello-Trampont, L.B. Haney, D. Klingele, J. Sondek, et al. 2004. PH domain of ELMO functions in trans to regulate Rac activation via Dock180. *Nat. Struct. Mol. Biol.* 11:756–762. http://dx.doi.org/10.1038/nsmb800

Marston, A.L., T. Chen, M.C. Yang, P. Belhumeur, and J. Chant. 2001. A localized GTPase exchange factor, Bud5, determines the orientation of division axes in yeast. *Curr. Biol.* 11:803–807. http://dx.doi.org/10.1016/S0960-9822(01)00230-5

Miller, P.J., and D.I. Johnson. 1997. Characterization of the *Saccharomyces cerevisiae* cdc42-1ts allele and new temperature-conditional-lethal cdc42 alleles. *Yeast*. 13:561–572. http://dx.doi.org/10.1002/(SICI)1097-0061(199705)13:6<561::AID-YEA114>3.0.CO;2-X

Moffat, J., and B. Andrews. 2004. Late-G1 cyclin-CDK activity is essential for control of cell morphogenesis in budding yeast. *Nat. Cell Biol.* 6:59–66. http://dx.doi.org/10.1038/ncb1078

Moskow, J.J., A.S. Gladfelter, R.E. Lamson, P.M. Pryciak, and D.J. Lew. 2000. Role of Cdc42p in pheromone-stimulated signal transduction in *Saccharomyces cerevisiae*. *Mol. Cell. Biol.* 20:7559–7571. http://dx.doi.org/10.1128/MCB.20.20.7559-7571.2000

Nern, A., and R.A. Arkowitz. 2000. Nucleocytoplasmic shuttling of the Cdc42p exchange factor Cdc24p. *J. Cell Biol.* 148:1115–1122. http://dx.doi.org/10.1083/jcb.148.6.1115

Okada, S., M. Leda, J. Hanna, N.S. Savage, E. Bi, and A.B. Goryachev. 2013. Daughter cell identity emerges from the interplay of Cdc42, septins, and exocytosis. *Dev. Cell*. 26:148–161. http://dx.doi.org/10.1016/j.devcel.2013.06.015

Ozbudak, E.M., A. Becskei, and A. van Oudenaarden. 2005. A system of counteracting feedback loops regulates Cdc42p activity during spontaneous cell polarization. *Dev. Cell*. 9:565–571. http://dx.doi.org/10.1016/j.devcel.2005.08.014

Pringle, J.R. 1991. Staining of bud scars and other cell wall chitin with calcofluor. *Methods Enzymol.* 194:732–735. http://dx.doi.org/10.1016/0076-6879(91)94055-H

Pringle, J.R., E. Bi, H.A. Harkins, J.E. Zahner, C. De Virgilio, J. Chant, K. Corrado, and H. Fares. 1995. Establishment of cell polarity in yeast. *Cold Spring Harb. Symp. Quant. Biol.* 60:729–744. http://dx.doi.org/10.1101/SQB.1995.060.01.079

Sanders, S.L., and I. Herskowitz. 1996. The BUD4 protein of yeast, required for axial budding, is localized to the mother/bud neck in a cell cycle-dependent manner. *J. Cell Biol.* 134:413–427. http://dx.doi.org/10.1083/jcb.134.2.413

Savage, N.S., A.T. Layton, and D.J. Lew. 2012. Mechanistic mathematical model of polarity in yeast. *Mol. Biol. Cell*. 23:1998–2013. http://dx.doi.org/10.1091/mbc.E11-10-0837

Schmidt, A., and A. Hall. 2002. Guanine nucleotide exchange factors for Rho GTPases: turning on the switch. *Genes Dev.* 16:1587–1609. http://dx.doi.org/10.1101/gad.1003302

Shimada, Y., M.-P. Gulli, and M. Peter. 2000. Nuclear sequestration of the exchange factor Cdc24 by Far1 regulates cell polarity during yeast mating. *Nat. Cell Biol.* 2:117–124. http://dx.doi.org/10.1038/35000073

Si, H., D. Justa-Schuch, S. Seiler, and S.D. Harris. 2010. Regulation of septum formation by the Bud3-Rho4 GTPase module in *Aspergillus nidulans*. *Genetics*. 185:165–176. http://dx.doi.org/10.1534/genetics.110.114165

Skotheim, J.M., S. Di Talia, E.D. Siggia, and F.R. Cross. 2008. Positive feedback of G1 cyclins ensures coherent cell cycle entry. *Nature*. 454:291–296. http://dx.doi.org/10.1038/nature07118

Slaughter, B.D., S.E. Smith, and R. Li. 2009. Symmetry breaking in the life cycle of the budding yeast. *Cold Spring Harb. Perspect. Biol.* 1:a003384. http://dx.doi.org/10.1101/cshperspect.a003384

Slaughter, B.D., J.R. Unruh, A. Das, S.E. Smith, B. Rubinstein, and R. Li. 2013. Non-uniform membrane diffusion enables steady-state cell polarization via vesicular trafficking. *Nat. Commun.* 4:1380. http://dx.doi.org/10.1038/ncomms2370

Smith, S.E., B. Rubinstein, I. Mendes Pinto, B.D. Slaughter, J.R. Unruh, and R. Li. 2013. Independence of symmetry breaking on Bem1-mediated autocatalytic activation of Cdc42. *J. Cell Biol.* 202:1091–1106. http://dx.doi.org/10.1083/jcb.201304180

Toenjes, K.A., M.M. Sawyer, and D.I. Johnson. 1999. The guanine-nucleotide-exchange factor Cdc24p is targeted to the nucleus and polarized growth sites. *Curr. Biol.* 9:1183–1186. http://dx.doi.org/10.1016/S0960-9822(00)80022-6

Wedlich-Soldner, R., S.C. Wai, T. Schmidt, and R. Li. 2004. Robust cell polarity is a dynamic state established by coupling transport and GTPase signaling. *J. Cell Biol.* 166:889–900. http://dx.doi.org/10.1083/jcb.200405061

Wu, C.F., and D.J. Lew. 2013. Beyond symmetry-breaking: competition and negative feedback in GTPase regulation. *Trends Cell Biol.* 23:476–483. http://dx.doi.org/10.1016/j.tcb.2013.05.003